Idelle Nono Kamga, Augustin Nkwento Nana, Bridget Ndoye Ndosiri, Frédéric Capet, Michel Foulon and Justin Nenwa*

The guanidinium *t*-diaqua-bis(oxalato) chromate(III) dihydrate complex: synthesis, crystal structure, EPR spectroscopy and magnetic properties

https://doi.org/10.1515/znb-2021-0006
Received January 19, 2021; accepted February 11, 2021; published online March 22, 2021

Abstract: A new salt $(CH_6N_3)[t\text{-}Cr(C_2O_4)_2(H_2O)_2]\cdot 2H_2O$ (**1**) ($CH_6N_3^+$ = guanidinium cation) has been synthesized and characterized by single-crystal X-ray diffraction, FT-IR and UV–Vis spectroscopies, elemental and thermogravimetric analyses. In the crystal structure of **1**, the chromate(III) ion lies on an inversion center in the form of an elongated octahedron. The coordination sphere consists of four oxygen atoms of two chelating oxalato ligands in the equatorial plane and two axial oxygen atoms of water ligands. The structural feature of focal interest in the structure of **1** is the formation of pillars of $[Cr(C_2O_4)_2(H_2O)_2]^-$ complex anions and $CH_6N_3^+$ guanidinium cations, with the next-neighbor cations rotated by an angle of 60° relative to each other. O–H···O and N–H···O hydrogen bonds play an important role in the construction of the three-dimensional network. The electron paramagnetic resonance (EPR) and magnetic properties of **1** have also been investigated.

Keywords: chromium(III) oxalate complex; crystal structure; EPR; guanidinium cation; magnetism.

1 Introduction

Organic–inorganic hybrid salts (OIHSs) represent an emerging class of crystalline materials formed by the self-assembly of organic cations and inorganic counterparts. In contrast to classical salts with rigid entities held together solely by electrostatic interactions, the flexibility offered by both the cationic and anionic entities provides to the family of OIHSs an opportunity to form unpredictable and interesting structures thanks to non-covalent interactions such as hydrogen bonding, π–π and/or van der Waals interactions [1–3]. Interest in OIHSs has been growing continuously over several decades owing to their fascinating structural architectures as well as their potential applications in catalysis [4], electronic and spintronic devices [5, 6], magnetism [7–9], and metallic conductivity [10]. Transition metal complexes provide useful anionic building blocks for the construction of OIHSs. In this context, the bis-oxalato complexes $[M^{III}(C_2O_4)_2(H_2O)_2]^-$, are extremely versatile building units for the synthesis of OIHSs, leading to two possible configurations: one, less common in the literature, in which the two H_2O ligands are *cis* to the equatorial plane formed by two chelating oxalato ligands [11–13] and another one, most common in the literature, in which the two H_2O ligands are *trans* to the equatorial plane [14–22]. Although several OIHSs of general formula A $[M^{III}(C_2O_4)_2(H_2O)_2]\cdot xH_2O$ (A^+ = iminium cations) have been explored to date, emphasis has been set on their structural aspects [11–22] and less attention has been paid to their magnetic properties as yet [21]. Taking this into account, in this contribution, we report the synthesis and characterization of a new Cr(III) hybrid salt $(CH_6N_3)[t\text{-}Cr(C_2O_4)_2(H_2O)_2]\cdot 2H_2O$ (**1**) ($CH_6N_3^+$ = guanidinium cation). The thermal stability, electron paramagnetic resonance (EPR) and magnetic properties of **1** have also been examined.

***Corresponding author: Justin Nenwa**, Inorganic Chemistry Department, University of Yaounde 1, P. O. Box 812, Yaounde, Cameroon, E-mail: jnenwa@yahoo.fr
Idelle Nono Kamga, Augustin Nkwento Nana and Bridget Ndoye Ndosiri, Inorganic Chemistry Department, University of Yaounde 1, P. O. Box 812, Yaounde, Cameroon
Frédéric Capet, Université de Lille, CNRS, Centrale Lille, Université Artois, UMR 8181 – UCCS – Unité de Catalyse et Chimie du Solide, F-59000 Lille, France
Michel Foulon, Département de Physique, Université de Lille, F-59650 Lille, Villeneuve d'Ascq, France

2 Results and discussion

The reaction of guanidinium carbonate with oxalic acid and chromium(III) chloride hexahydrate in a molar ratio of 0.5:2:1 in water produced red prismatic crystals of salt **1**

with 85% yield. Salt **1** is air-stable and does not melt below 300 °C.

2.1 IR and UV–Vis spectra of salt 1

The IR spectrum of **1** between 400 and 4000 cm^{-1} is shown in Figure S1 (Supplementary Material, available online). The broad absorption bands around 3434 and 3286 cm^{-1} are attributed to ν(N–H) and ν(O–H), respectively. The band centered at 1659 cm^{-1} is due to ν(C=O), and the bands centered at 1393 and 1267 cm^{-1} are attributed to ν(C–O) [23]. The bands centered at 900 and 814 cm^{-1} are assigned to νC–C. The sharp bands observed at 480 and 408 cm^{-1} are due to Cr–O vibrations [24].

The UV–Vis spectrum of **1** is shown in Figure S2 (Supplementary Material). It exhibits two bands in the visible region, one at 415 nm and the other at 561 nm due to *d*–*d* transitions, $^4A_{2g} \rightarrow {}^4T_{1g}(F)$ and $^4A_{2g} \rightarrow {}^4T_{2g}$, respectively. These results are in accordance with reported values [21, 25–27].

2.2 Description of the crystal and molecular structure of salt 1

Single-crystal X-ray structural analysis has shown that crystals of compound **1** belong to the monoclinic system with the space group *C*2/*c* and *Z* = 4 (Table 1). As highlighted in Figure 1a, the structure of **1** consists of one *trans*-diaquabis(oxalato)chromate(III) $[Cr(C_2O_4)_2(H_2O)_2]^-$ complex anion, one $CH_6N_3^+$ guanidinium cation compensating the charge of the anion, and two uncoordinated water molecules. In the anionic complex, the six-coordinated Cr^{III} ion lies on a crystallographic inversion center and the coordination sphere involves four O atoms from two chelating oxalate dianions [Cr–O1, 1.9611(6) Å, Cr–O1^i, 1.9611(6) Å, Cr–O4, 1.9624(5) Å, Cr–O4^i, 1.9624(5) Å] and two O atoms of *trans*-related water molecules [Cr–O5, 1.9854(7) Å, Cr–O5^i, 1.9854(7) Å]. The Cr–O_{water} distance [1.9854(7) Å] is longer than those of the Cr–$O_{oxalate}$ bonds (Table 2). These parameters indicate a slightly elongated octahedron around the Cr^{III} ion. These bond lengths are comparable with the values reported for salts containing the $[Cr(C_2O_4)_2(H_2O)_2]^-$ complex anion in *trans* configuration [14–16, 21, 22]. It is worth noting that the imidazolium salt $(C_3H_5N_2)[t\text{-}Cr(C_2O_4)_2(H_2O)_2]\cdot 2H_2O$ [22] and the present guanidinium salt $(CH_6N_3)[t\text{-}Cr(C_2O_4)_2(H_2O)_2]\cdot 2H_2O$ are isotypic and they exhibit very similar basic structures except for the distinction of cationic entities. In both salts, each complete cation is generated by a crystallographic twofold rotation axis, with a carbon atom lying on the rotation axis. The bond lengths [C3–N1 1.3166(9) Å, C3–N1^{ii} 1.3166(9) Å, C3–N2 1.3263(17) Å] and angles [N2–C3–N1 119.85(6)°, N2–C3–N1^{ii} 119.85(6)°, N1–C3–N1^{ii} 120.30(12)°] (symmetry code: (ii) $-x+1, y, -z+3/2$) in the $CH_6N_3^+$ guanidinium cation show no significant difference from those observed in other guanidinium salts [28–30].

The structural feature of focal interest in **1** is the formation of pillars of $[Cr(C_2O_4)_2(H_2O)_2]^-$ complex anions and $CH_6N_3^+$ guanidinium cations, with the next-neighbor cations rotated by an angle of 60° relative to each other (Figure 1b). The intermetallic Cr···Cr distances vary in the range of 6.4561(2)–9.8555(4) Å. The 3D supramolecular architecture of **1** (Figure 2, Table 3) is stabilized through a network of intermolecular hydrogen bonding interactions: N–H···O [2.867(10)–3.017(9) Å] hydrogen bonds linking guanidinium cations and $[Cr(C_2O_4)_2(H_2O)_2]^-$

Table 1: Crystal data and numbers pertinent to data collection and structure refinement of **1**.

Compound	**1**
Empirical formula	$C_5H_{14}CrN_3O_{12}$
Formula weight	360.19
T, K	296
λ, Å	0.71073
Crystal system	monoclinic
Space group	*C*2/*c* (#15)
a, Å	10.5692(5)
b, Å	7.4174(4)
c, Å	16.2592(8)
β, deg	92.076(2)
V, Å^3	1273.82(11)
Z	4
D_{calcd}, g cm^{-3}	1.878
μ, mm^{-1}	1.0
F(000), *e*	740
Crystal size, mm^3	0.32 × 0.18 × 0.17
θ range data collection, deg	2.5–36.2
Index ranges *hkl*	±17, ±12, ±27
Total reflections	47,107
Unique reflections/R_{int}	3084/0.029
Refinement method	full-matrix least-squares on F^2
Data/refined parameters	3084/127
R_1/wR_2[a,b] [$I > 2\sigma(I)$]	0.023/0.067
R_1/wR_2[a,b] (all data)	0.026/0.101
A/*B* (weight *w*)[b]	0.0352/0.493
Goodness-of-fit[c] (GoF) on F^2	1.08
$\Delta\rho_{fin}$ (max/min), *e* Å^{-3}	0.38/−0.43

[a] $R_1 = \Sigma||F_o|-|F_c||/\Sigma|F_o|$; [b] $wR_2 = [\Sigma w(F_o^2-F_c^2)^2/\Sigma w(F_o^2)^2]^{1/2}$, $w = [\sigma^2(F_o^2)+(AP)^2+BP]^{-1}$, where $P = (\mathrm{Max}(F_o^2, 0)+2F_c^2)/3$; [c] $\mathrm{GoF} = S = [\Sigma w(F_o^2-F_c^2)^2/(n_{obs}-n_{param})]^{1/2}$.

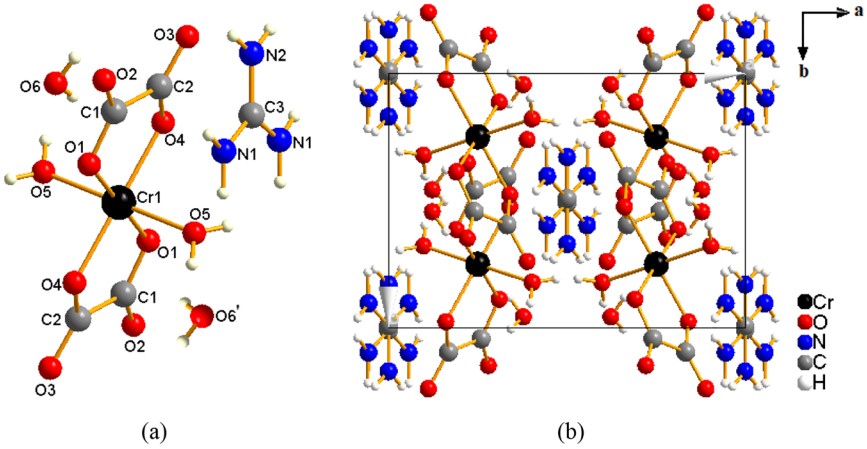

Figure 1: (a) Constitutive entities of **1** with atom numbering scheme. (b) Packing diagram of **1** highlighting pillars of the $[Cr(C_2O_4)_2(H_2O)_2]^-$ complex anions and guanidinium $CH_6N_3^+$ cations, with the next-neighbor cations rotated by an angle of 60° relative to each other.

Table 2: Selected bond lengths (Å) and angles (deg) for compound **1**.[a]

Cr1–O4	1.9624(5)	O1^i–Cr1–O1	180
Cr1–O4^i	1.9624(5)	O4^i–Cr1–O4	180
Cr1–O1	1.9611(6)	O5–Cr1–O5^i	180
Cr1–O1^i	1.9611(6)	O1–Cr1–O5	90.99(3)
Cr1–O5^i	1.9854(7)	O1–Cr1–O4	82.94(2)
Cr1–O5	1.9854(7)	O4–Cr1–O5	93.11(3)

[a]Symmetry code: (i) $-x + 1/2, -y + 3/2, -z + 1$.

complex anions and O–H···O [2.643(10) Å] hydrogen bonds linking coordinated water molecules and crystallization water molecules.

2.3 PXRD and thermogravimetric analysis of salt 1

The phase purity of **1** can be proven by powder X-ray diffraction (PXRD) analysis. As shown in Figure S3 (Supplementary Material), the PXRD pattern of the bulk sample is in good agreement with the pattern simulated from the single-crystal data.

Results of the thermal analyses (Thermogravimetric analysis, TGA and Differential scanning calorimetry, DSC) of a powder sample of **1** is depicted in Figure 3. The TGA curve shows three main decomposition steps. In the range of 100–140 °C, a first weight loss of 10.1%, associated with an endothermic effect, corresponds to the release of two water molecules of crystallization (calcd. 10.0%) to give the anhydrous derivative $(CH_6N_3)[Cr(C_2O_4)_2(H_2O)_2]$. In the range of 200–240 °C, a second weight loss of 11.7%, associated with an endothermic effect, is ascribed to the decomposition of the guanidinium cation (calcd. 11.7%), leading to the release of CH_2N_2 [31] and formation of the intermediate $(NH_4)[Cr(C_2O_4)_2(H_2O)_2]$. In the range of 340–360 °C, the latter intermediate undergoes a weight loss of 66.2% associated with an exothermic effect, leading to the decomposition of the framework (calcd. 66.1%) and formation of a dark-green residue which has been proven to be Cr_2O_3.

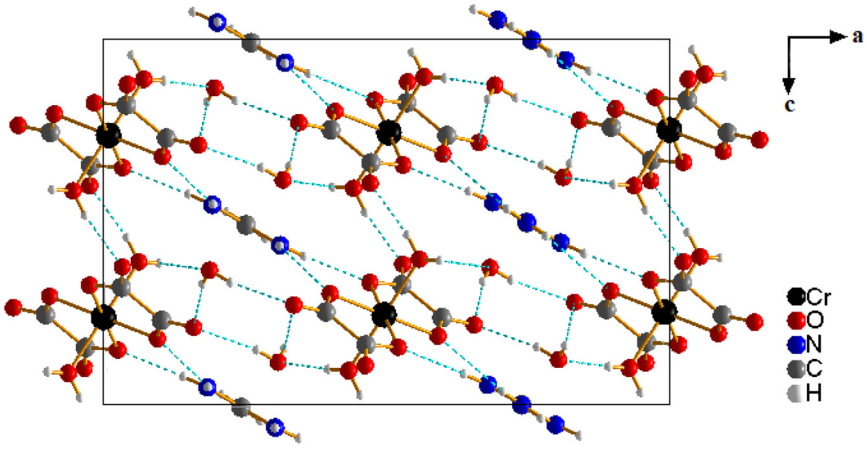

Figure 2: View of the three-dimensional supramolecular structure of **1**. The dashed lines show hydrogen bonding interactions.

Table 3: Hydrogen bonding interactions (Å, deg) for compound **1**.[a]

D–H···*A*	*D*–H	H···*A*	*D*···*A*	*D*–H···*A*
N1–H1*A*···O1^{i}	0.897(19)	2.371(19)	2.948(10)	122.2(15)
N2–H2···O2^{iv}	0.812(19)	2.280(2)	3.017(9)	150(2)
O5–H5*A*···O6	0.843(17)	1.809(17)	2.642(10)	170.0(17)
O5–H5*B*···O3^{v}	0.79(2)	1.920(2)	2.691(9)	168(2)
O6–H6*A*···O3^{iv}	0.729(18)	2.601(18)	2.999(10)	116.6(16)
O6–H6*A*···O2^{iv}	0.729(18)	2.142(19)	2.865(10)	171.4(19)
N1–H1*B*···O4	0.873(19)	2.060(19)	2.867(10)	153.4(17)
O6–H6*B*···O2^{vi}	0.792(19)	2.221(19)	3.004(10)	170.1(17)

[a]Symmetry codes: (i) $-x + 1/2, -y + 3/2, -z + 1$; (iv) $-x + 1/2, -y + 1/2, -z + 1$; (v) $x - 1/2, y + 1/2, z$; (vi) $x, -y + 1, z + 1/2$.

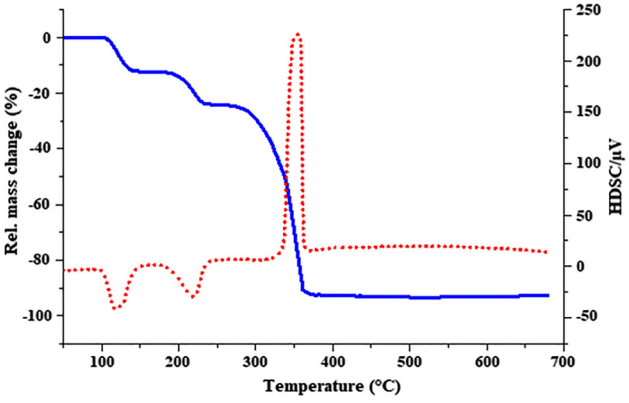

Figure 3: TGA (blue) and DSC (red) diagrams for **1**.

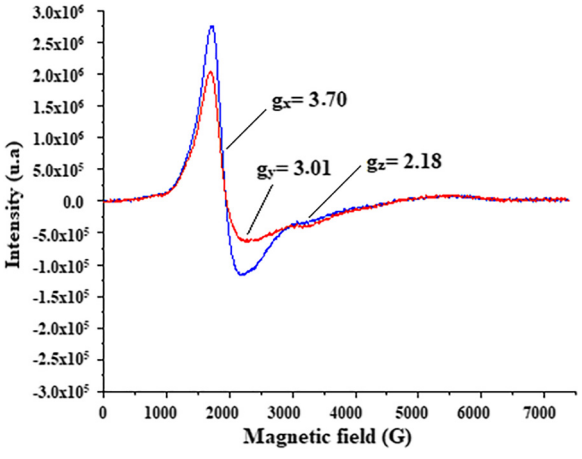

Figure 4: Experimental (blue) and simulated (red) X-band EPR spectra for **1**.

2.4 EPR spectrum and magnetic properties

The experimental EPR spectrum of a powdered sample of **1** with the resulting parameters measured at room temperature (blue curve) and a simulated EPR spectrum (red curve) are displayed in Figure 4. The two spectra are practically superimposable. The anisotropy of the g parameters along the three principal axes are: g_x = 3.70, g_y = 3.01 and g_z = 2.18. The g anisotropy with three different Eigen values is in accordance with a distortion of the octahedral environment around the chromium(III) complex in **1** [32–34].

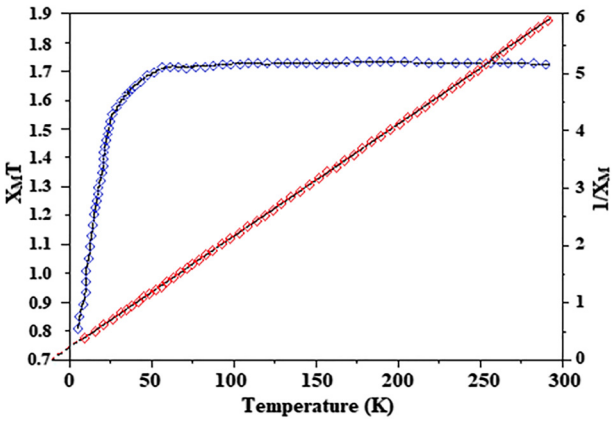

Figure 5: Temperature dependences of X_MT and X_M^{-1} for **1**.

Magnetic susceptibilities of **1** were measured from 300 to 2 K in a magnetic field of 0.1 T. The temperature dependences of X_MT and X_M^{-1} (χ_M is the molar magnetic susceptibility) are depicted in Figure 5.

At room temperature, the value of X_MT is ca. 1.74 cm^3 K mol^{-1} which is not far from the expected value (1.87 cm^3 K mol^{-1}) for magnetically isolated Cr(III) centers. Upon cooling, the product X_MT remains practically constant down to 50 K, then it decreases more and more rapidly reaching 0.80 cm^3 K mol^{-1} at 2 K. The temperature dependence of X_M^{-1} above 50 K obeys the Curie–Weiss equation $X_M^{-1} = (T - \theta)/C$ with the Curie–Weiss constants C = 4.56 cm^3 K mol^{-1}, θ = –10.07 K. The negative value of θ and the decrease of X_MT at lower temperatures may be attributed to the zero-field splitting (ZFS) effects associated with the axially elongated Cr(III) ion or to weak antiferromagnetic intermolecular interactions between the Cr(III) spin carriers or to both factors simultaneously [21, 35].

3 Conclusion

In summary, a new Cr(III) complex with oxalate ligands with guanidinium as counter cation has been synthesized and structurally and magnetically characterized. In the

Cr(III) complex, the Cr(III) ions are hexacoordinated by four O atoms of two chelating oxalato ligands and two coordinated water molecules in *trans* configuration. Thermal studies confirmed the presence of crystal water in **1**. The observed EPR spectrum is in accordance with the simulation and strongly supports the Cr(III) oxidation state in an octahedral environment. Temperature-dependent molar susceptibility measurements suggest the occurrence of weak antiferromagnetic interactions between the Cr(III) ions. This work not only enriches the family of bis(oxalato) metalate(III) hybrid salts involving iminium cations, but also may be a useful reference for designing other homologous materials with respect to their solid-state magnetic properties.

4 Experimental section

4.1 Materials and physical measurements

All chemicals were of analytical reagent grade and were used without further purification. Elemental analyses for C, H and N were carried out a Fisons-EA 1108 CHN analyzer. The infrared (IR) spectrum of compound **1** was recorded on a Perkin-Elmer 2000 FT-IR spectrometer using KBr pellets in the range of 4000–400 cm^{-1}. The UV–Vis spectrum was obtained on a Bruker HACH DR 3900 spectrophotometer, in water, in the range 300–800 nm. X-ray powder measurements were performed at room temperature. Data were collected on a Bruker D8 Advance A25 diffractometer, in Bragg–Brentano geometry, using CuKα radiation. The simulation from the single-crystal data was performed with the Mercury software [36]. TGA was carried out on a LINSEIS STA PT-1000 thermal analyzer. The powdered sample (20 mg) was heated from 25 to 700 °C with a rate of 10 K min^{-1} in an air flow. The EPR spectrum was recorded using a Bruker ELEXYS E500 spectrometer operating at 9 GHz at room temperature. The spectrum was simulated with the program WinEPR SimFonia by Bruker [37]. Magnetic susceptibility data were performed on a Quantum Design MPMS-5XL SQUID magnetometer in the temperature range 2–300 K at an applied magnetic field of 0.1 T.

4.2 Synthesis of $(CH_6N_3)[t\text{-}Cr(C_2O_4)_2(H_2O)_2]\cdot 2H_2O$ (1)

A mixture of guanidinium carbonate $(CH_6N_3)_2CO_3$ (90 mg; 0.5 mmol) and oxalic acid dihydrate $H_2C_2O_4\cdot 2H_2O$ (252 mg; 2 mmol) was added in small portions to a stirred green aqueous solution of chromium trichloride hexahydrate $CrCl_3\cdot 6H_2O$ (266 mg; 1 mmol) at 70 °C. After 2 h of stirring in air under ambient conditions, the reaction mixture was gradually cooled to room temperature and filtered. The purple filtrate was allowed to evaporate in a hood at room temperature. Three weeks later, red prismatic crystals suitable for X-ray diffraction were isolated with a yield of 85% based on $(CH_6N_3)_2CO_3$ – Elemental analysis calcd. for $C_5H_{14}CrN_3O_{12}$ (M_r = 360.19): C 16.67, H 3.92, N 11.67; found C 16.51, H 4.01, N 11.56%.

4.3 Crystallographic data collection and structure refinement

A suitable single crystal of dimensions $0.32 \times 0.18 \times 0.17$ mm^3 was selected for indexing, and the intensity data were recorded at 296 K on a Bruker APEX II CCD diffractometer equipped with a Mo Incoatec Microfocus Source IμS (λ = 0.71073 Å). Using Olex2 [38], the structure of **1** was solved with the program Shelxt [39] by using the intrinsic phasing solution method. The model was refined with Shelxl-2018/3 [40] using least-squares minimization. All nonhydrogen atoms were refined anisotropically and all H atoms linked to N and O atoms were located from the electron density difference map and refined freely. The crystallographic data and structure refinement details are summarized in Table 1, and selected bond lengths and angles are listed in Table 2.

CCDC 2040246 contains supplementary crystallographic data for **1**. These data can be obtained free of charge from The Cambridge Crystallographic Data Center *via* www.ccdc.cam.ac.uk/data_request/cif.

5 Supporting information

The IR and UV/Vis spectra, the experimental and simulated PXRD patterns of compound **1** are given as supplementary material available online (https://doi.org/10.1515/znb-2021-0006).

Acknowledgements: The authors thank Dr. Pascal Roussel (UCCS) and Dr. Hervé Vezin (LASIRE), (Research Directors at the CNRS), for their assistance with the PXRD and the magnetic measurements, respectively. Chevreul Institute (FR 2638), Ministère de l'Enseignement Supérieur, de la Recherche et de l'Innovation, Région Hauts de France and FEDER are acknowledged for supporting and funding partially this work.

Author contribution: All the authors have accepted responsibility for the entire content of this submitted manuscript and approved submission.
Research funding: This study was funded by Chevreul Institute (FR 2638), Ministère de l'Enseignement Supérieur, de la Recherche et de l'Innovation, Région Hauts de France and FEDER.
Conflict of interest statement: The authors declare no conflicts of interest regarding this article.

References

1. Gamble F. R., DiSalvo F. J., Klemm R. A., Geballe T. H. *Science* 1970, *168*, 568–570.
2. Reineke T. M., Eddaoudi M., Moler D., O'Keeffe M., Yaghi O. M. *J. Am. Chem. Soc.* 2000, *122*, 4843–4844.
3. Zhang B., Zhang Y., Wang Z., Gao S., Guo Y., Liu F., Zhu D. *Cryst. Eng. Comm.* 2013, *15*, 3529–3535.
4. Yaghi O. M., O'Keeffe M., Ockwig N. W., Chae H. K., Eddaoudi M., Kim J. *Nature* 2003, *423*, 705–714.
5. Coronado E., Day P. *Chem. Rev.* 2004, *104*, 5419–5448.
6. Pedersen A. H., Julve M., Martínez-Lillo J., Cano J., Brechin E. K. *Dalton Trans.* 2017, *46*, 16025–16033.
7. Kahn O. *Angew. Chem. Int. Ed.* 1985, *24*, 834–850.
8. Clemente-Leon M., Coronado E., Marti-Gastaldo C., Romero F. M. *Chem. Soc. Rev.* 2011, *40*, 473–497.
9. Zhang B., Zhang Y., Zhu D. *Dalton Trans.* 2012, *41*, 8509–8511.
10. Mitzi D. B., Wang S., Field C. A., Chess C. A., Guloy A. M. *Science* 1995, *267*, 1473–1476.
11. Chérif I., Abdelhak J., Zid M. F., Driss A. *Acta Crystallogr.* 2012, *E68*, m824–m825.
12. Nenwa J., Befolo O., Gouet B., Mbarki M., Fokwa B. P. T. *Acta Crystallogr.* 2012, *E68*, m1434–m1441.
13. Djomo E. D., Capet F., Nenwa J., Bélombé M. M., Foulon M. *Acta Crystallogr.* 2015, *E71*, 934–936.
14. Bélombé M. M., Nenwa J., Emmerling F. Z. *Z. Kristallogr. N. Cryst. Struct.* 2009, *224*, 239–240.
15. Nenwa J., Belombe M. M., Ngoune J., Fokwa B. P. T. *Acta Crystallogr.* 2010, *E66*, m1410–m1418.
16. Chérif I., Abdelhak J., Zid M. F., Driss A. *Acta Crystallogr.* 2011, *E67*, m1648–m1649.
17. Chérif I., Zid M. F., El-Ghozzi M., Avignant D. *Acta Crystallogr.* 2012, *E68*, m900–m901.
18. Nenwa J., Bebga G., Signé M., Bélombé M. M., Mbarki M., Fokwa B. P. T. *Acta Crystallogr.* 2012, *E68*, m1325–m1326.
19. Dridi R., Namouchi C. S., Zid M. F., Driss A. *Acta Crystallogr.* 2013, *E69*, m489–m490.
20. Bebga G., Signé M., Nenwa J., Mbarki M., Fokwa B. P. T. *Acta Crystallogr.* 2013, *E69*, m567–574.
21. Chérif I., Abdelhak J., Amami M., Hlil E. K., Zid M. F., Driss A. *QSci. Connect* 2013, *46*, 10.
22. Chérif I., Abdelhak J., Zid M. F., Driss A. *Acta Crystallogr.* 2013, *E69*, m667–m668.
23. Nanda P. K., Ray D. *Inorg. Chim. Acta.* 2005, *358*, 4039–4044.
24. Bellamy L. J. *Infrared Spectra of Complex Molecules*; Chapman & Hall: New York, 1980.
25. Decurtins S., Schmalle H. W., Oswald H. R., Linden A., Ensling J., Gütlich P., Hauser A. *Inorg. Chim. Acta.* 1994, *216*, 65–73.
26. Roy A., Nag K. *J. Inorg. Nucl. Chem.* 1978, *40*, 1501–1505.
27. Bélombé M. M., Nenwa J., Mbiangué Y. A., Bebga G., Majoumo-Mbé F., Hey-Hawkins E., Lönnecke P. *Inorg. Chim. Acta.* 2009, *362*, 1–4.
28. Golic L., Bulc N. *Acta Crystallogr.* 1988, *C44*, 2065–2068.
29. Boghaei D. M., Najafpour M. M. *Anal. Sci.* 2007, *23*, x123–x124.
30. Nenwa J., Djomo E. D., Nfor E. N., Djonwouo P. L., Mbarki M., Fokwa B. P. T. *Polyhedron* 2015, *99*, 26–33.
31. Thomas Y., Taravel B., Fromage F., Delorme P. *Mater. Chem.* 1980, *5*, 117–123.
32. Prokhorova T. G., Khasanov S. S., Zorina L. V., Buravov L. I., Tkacheva V. A., Baskakov A. A., Morgunov R. B., Gener M., Canadell E., Shibaeva R. P., Yagubskii E. B. *Adv. Funct. Mater.* 2003, *13*, 403–411.
33. Nana A. N., Haynes D., Vezin H., Minaud C., Shankhari P., Fokwa B. P. T., Nenwa J. *J. Mol. Struct.* 2020, *1220*, 128642–128650.
34. Choubeu C. M. N., Ndosiri B. N., Vezin H., Minaud C., Orton J. B., Coles S. J., Nenwa J. *Polyhedron* 2021, *193*, 114885–114892.
35. Kahn O. *Molecular Magnetism*; VCH Publishers: New York, 1993.
36. Macrae C. F., Edgington P. R., McCabe P., Pidcock E., Shields G. P., Taylor R., Towler M., DeStreek J. V. *J. Appl. Crystallogr.* 2006, *39*, 453–457.
37. Weber R. T. WinEPR SimFonia (version 1.2); EPR Division, Bruker Instruments Inc.: Billerica, 1995.
38. Dolomanov O. V., Bourhis L. J., Gildea R. J., Howard J. A. K., Puschmann H. *J. Appl. Crystallogr.* 2009, *42*, 339–341.
39. Sheldrick G. M. *Acta Crystallogr.* 2015, *A71*, 3–8.
40. Sheldrick G. M. *Acta Crystallogr.* 2015, *C71*, 3–8.

Supplementary Material: The online version of this article offers supplementary material (https://doi.org/10.1515/znb-2021-0006).